nanomaterials

MDPI

Review

Electrolyte Effect on Electrocatalytic CO_2 Reduction

Jiandong Zhang [1,*], Ziliang Zhang [2], Tianye Chen [3], Jiayi Zhang [3] and Yu Zhang [1,*]

[1] College of Civil Engineering and Architecture, Zhejiang University, Hangzhou 310058, China
[2] School of Electro-Mechanical Engineering, Guangdong University of Technology, Guangzhou 510006, China; 3122000399@mail2.gdut.edu.cn
[3] Faculty of Mechanical Engineering and Mechanics, Ningbo University, Ningbo 315211, China; 236001862@nbu.edu.cn (T.C.); 236003994@nbu.edu.cn (J.Z.)
* Correspondence: zhangjd_7@zju.edu.cn (J.Z.); zhangyu0203@zju.edu.cn (Y.Z.)

Abstract: Electrocatalytic CO_2 reduction reaction shows great potential for converting CO_2 into high-value chemicals and fuels at normal temperature and pressure, combating climate change and achieving carbon neutrality goals. However, the complex reaction pathways involve the transfer of multiple electrons and protons, resulting in poor product selectivity, and the existence of competitive hydrogen evolution reactions further increases the associated difficulties. This review illustrates the research progress on the micro mechanism of electrocatalytic CO_2 reduction reaction in the electrolyte environment in recent years. The reaction pathways of the products, pH effects, cation effects and anion effects were systematically summarized. Additionally, further challenges and difficulties were also pointed out. Thus, this review provides a theoretical basis and future research direction for improving the efficiency and selectivity of electrocatalytic CO_2 reduction reaction.

Keywords: electrocatalytic CO_2 reduction; pH effects; cation effects; anion effects

check for updates

Academic Editor: Antonio Guerrero-Ruiz

Received: 22 March 2025
Revised: 16 April 2025
Accepted: 23 April 2025
Published: 25 April 2025

Citation: Zhang, J.; Zhang, Z.; Chen, T.; Zhang, J.; Zhang, Y. Electrolyte Effect on Electrocatalytic CO_2 Reduction. *Nanomaterials* **2025**, *15*, 648. https://doi.org/10.3390/nano15090648

1. Introduction

Electrocatalytic CO_2 reduction reaction (CO_2RR) has exhibited immense potential as a promising solution to address climate change by converting CO_2 into high-value chemicals and fuels, a process that can be carried out under ambient temperature and pressure with adjustable reactants and driven by renewable energy sources such as wind and solar power [1–4]. Nevertheless, the reduction pathways are intricate and involve multiple electron (i.e., e^-) and proton (i.e., H^+) transfers, leading to low selectivity. Additionally, the competing hydrogen evolution reaction (HER) presents a significant challenge in realizing high local current density and faradaic efficiency (FE) [5,6]. Thus, the development of efficient electrocatalytic reduction technologies is of great practical significance.

The electrocatalytic CO_2RR occurs within the electrical double layer (EDL) at the electrode–electrolyte interface (EEI), so its efficiency relies not only on the electrode materials (i.e., catalysts) but also on the electrolyte. Previous studies have primarily concentrated on the optimization of catalysts, such as enhancing catalytic performance through morphology and facet engineering [7,8], vacancy steering [9], doping modification [10,11], alloying [12] and single-atom sites [13–15]. These strategies increase the number of active sites on the catalyst surface, alter the material electronic structure and local charge polarization or realize synergistic effects between multiple components, optimizing the adsorption or desorption reactions of intermediates and charge transfer process. Despite advancements, only Cu-based catalysts have been proven to reduce CO_2 to multi-carbon products, but the activity remains low [16–18]. Consequently, merely depending on catalyst

optimization may not fully resolve the challenges faced by CO_2RR. In this context, as an indispensable part of the reaction, the electrolyte has also gained much attention, not only providing protons but also directly affecting the formation of intermediates and the reaction pathway [19–23]. As outlined in Figure 1, the variation of the reaction pathway is first summarized to understand how the electrolyte influences product selectivity, then the electrolyte's effects are extensively studied, including pH effects [24–26], cation effects [27–31], and anion effects [32–34]. Nevertheless, despite immense achievements, the specific effect may differ across studies, resulting in limited consensus. For instance, due to the coexistence of cations and anions at the EEI, multi-interactions overcomplicate related research. Buffer ions are generally introduced to control pH, which leads to confusion between the effects of pH and ions, making it challenging to isolate their individual contributions [23]. Thus, this field lacks a critical and systemic synthesis to summary conflicting observations and the underlying causes of discrepancies in electrolyte effects.

Unlike previous reviews that primarily catalog electrolyte effects [35–37], this work critically examines the contradictions among existing studies and identifies key factors (e.g., interfacial field screening, buffer-induced artifacts, and ion cooperativity) that lead to divergent conclusions. By establishing a mechanistic framework that disentangles these complexities, this work provides not only a unified perspective but also practical guidelines for future experimental design—a step toward resolving long-standing debates in CO_2RR electrolyte engineering.

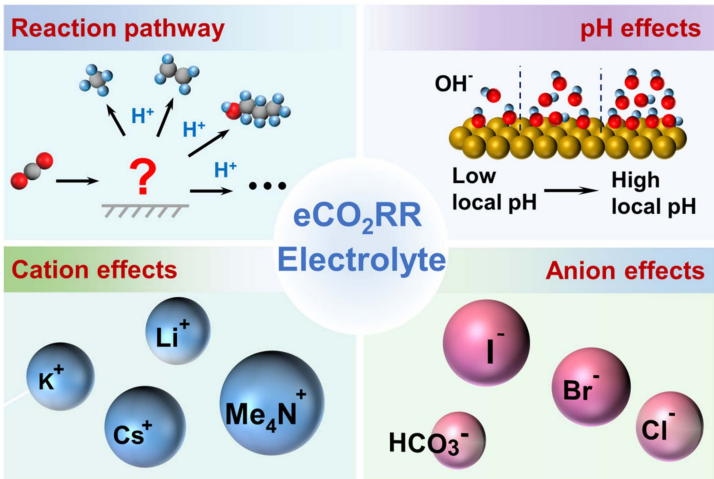

Figure 1. The overview diagram of the content of the review. The variation of the reaction pathway is first summarized to understand how the electrolyte influences product selectivity. Then, the effects of pH, cations and anions are reviewed. Note, the red "?" represents the possible reaction pathways.

2. Reaction Pathway

Proton-coupled electron transfer (PCET) processes occur in CO_2RR,* and the number of electrons involved in the reaction may vary depending on the catalyst and reaction conditions, typically ranging from $2e^-$, $4e^-$, $6e^-$, and $8e^-$ to $12e^-$ or even more [23]. The difference in electron number directly determines the type of reduced products [18], as shown in Table 1. The products of CO_2RR include carbon monoxide (CO), formic acid (HCOOH) and formate ($HCOO^-$), oxalic acid ($H_2C_2O_4$) and oxalate ($C_2O_4^{2-}$), methane (CH_4), formaldehyde (CHOH), methanol (CH_3OH), ethylene (C_2H_4) and ethanol (C_2H_5OH) [7,38–41]. All products begin with the adsorption of CO_2 on the catalyst surface to $*CO_2$ intermediate (* indicates an active site), and the configuration of $*CO_2$ largely determines the reaction pathway. As shown in Figure 2a, the proton–electron transfer occurs via two pathways [42]. The blue arrow represents the sequential proton–electron transfer (SPET), where the $*CO_2$

first accepts an electron to form $*CO_2^-$ with the carbon coordinated to the catalyst, and then accepts a proton to form *COOH (a key precursor to *CO). The green arrow represents the concerted proton–electron transfer (CPET), where the $*CO_2$ directly gains both a proton and an electron to form *COOH [43]. *CO can desorb from the catalyst surface to generate CO (Product I), so the pathway can be described as follows: $*CO_2 \rightarrow *COOH \rightarrow *CO \rightarrow CO$. Apart from *COOH, based on the $*CO_2$ configuration, CO_2 can also be hydrogenated to HCOO*, ultimately generating HCOOH (Product II) or $HCOO^-$ (Product III) [44]. Other product pathways are depicted in Figure 2b. HCHO (Product IV), CH_3OH (Product V) and CH_4 (Product VI) are also common C_1 products, which involve $4e^-$, $6e^-$, and $8e^-$ electron transfer. Intricately, competing reactions exist between different products, such as the intermediates for HCHO and CH_3OH being *CHO. The intermediates also vary depending on the catalyst surface and reaction conditions. For instance, Shi et al. [42] described that *COH can directly dehydrate to *C, then be further hydrogenated to CH_4. However, other studies suggest that *COH first combines with H to *CHOH, which then undergoes dehydration to form *CH, followed by proton coupling to generate CH_4 [45,46].

Table 1. The reactions of CO_2RR and HER [18]. Copyright 2019, American Chemical Society.

Reaction	Potential (V vs. RHE)
$x\ CO_2 + n\ H^+ + n\ e^- \rightarrow product + y\ H_2O$	
$CO_2 + 2H^+ + 2e^- \rightarrow CO\ (g) + H_2O$	−0.10
$CO_2 + 2H^+ + 2e^- \rightarrow HCOOH\ (aq)$	−0.12
$CO_2 + 4H^+ + 4e^- \rightarrow C\ (s) + 2H_2O$	0.21
$CO_2 + 6H^+ + 6e^- \rightarrow CH_3OH\ (aq) + H_2O$	0.03
$CO_2 + 8H^+ + 8e^- \rightarrow CH_4\ (aq) + 2H_2O$	0.17
$2CO_2 + 8H^+ + 8e^- \rightarrow CH_3COOH\ (aq) + 2H_2O$	0.11
$2CO_2 + 10H^+ + 10e^- \rightarrow CH_3CHO\ (aq) + 3H_2O$	0.06
$2CO_2 + 12H^+ + 12e^- \rightarrow C_2H_4\ (q) + 4H_2O$	0.08
$2CO_2 + 12H^+ + 12e^- \rightarrow C_2H_5COOH\ (aq) + 3H_2O$	0.09
$2CO_2 + 14H^+ + 14e^- \rightarrow C_2H_6\ (g) + 4H_2O$	0.14
$3CO_2 + 16H^+ + 16e^- \rightarrow C_2H_5CHO\ (aq) + 5H_2O$	0.09
$3CO_2 + 18H^+ + 18e^- \rightarrow C_3H_7OH\ (aq) + 5H_2O$	0.10
$H_3O^+ \rightarrow H^+ + H_2O$	-
$2H^+ + 2e^- \rightarrow H_2$	0
$2H_2O + 2e^- \rightarrow H_2 + 2OH^-$	-

Multi-carbon products involve more proton–electron transfer and follow complex reaction pathways. Figure 2b summarizes a series of possible multi-carbon products, including C_2H_4, CH_3CH_2OH, ethane (C_2H_6), ethylene glycol ($C_2H_6O_2$), acetic acid (CH_3COOH) and propanol (C_3H_7OH) [42,46–50]. *CO is considered a key intermediate for C_2 products, and the C-C coupling is the RLS [51]. The widely accepted pathway is that *CO undergoes C-C coupling to generate C_2 products (e.g., $*CO + *CO \rightarrow *OCCO$). Taking the generation pathway of C_2H_4 as an example, Qiu et al. [52] proposed that C_2H_4 formation requires combining CO and *CHO to create *COCHO, then the two carbon atoms hydrogenate and deoxygenate to *CCH, which is further hydrogenated to form C_2H_4. However, an alternative view is that *CO and *CO directly undergo C-C coupling to form *OCCO [53]. In this pathway, the coupled C atoms undergo hydrogenation and deoxygenation to form *CCO, which then proceeds through PCET steps to generate CHCO, CHCHO, CH_2CHO, and ultimately C_2H_4. Thus, exploring the universality of reaction pathways remains a critical focus, and studies on the mechanisms of multi-carbon products are still limited, requiring further exploration and validation.

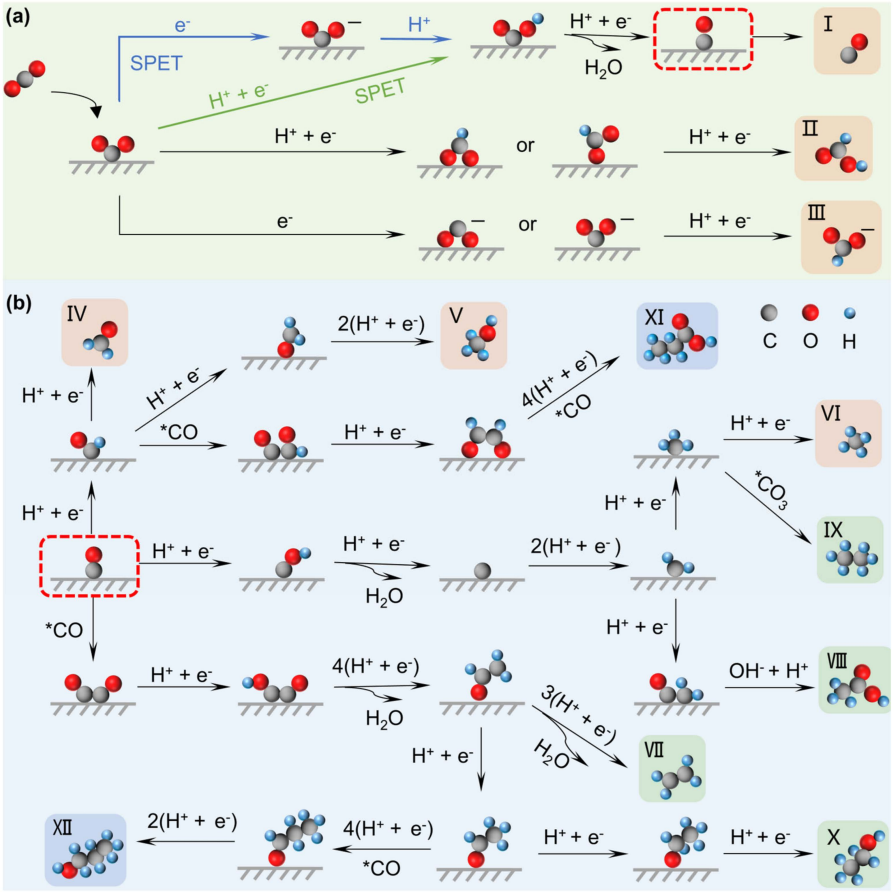

Figure 2. (**a**) Two pathways of electron transfer, and (**b**) overview of reaction pathways for CO_2RR towards different products [42]. Copyright 2024, Elsevier.

3. pH Effects

The selectivity of CO_2RR is significantly influenced by the electrolyte pH, with the main difference between acidic and neutral/alkaline electrolytes being the proton source. As shown in Table 1, in acidic media, hydrated hydrogen ions (H_3O^+) act as the proton source, while water molecules serve as proton donors in neutral/alkaline electrolytes [54,55]. Typically, CO_2RR is conducted in neutral or alkaline electrolytes, since a higher pH helps suppress the competing HER [26,56]. However, some studies indicate that HER at the reversible hydrogen electrode (RHE) is independent of pH, as it can be driven by the reduction of water molecules [18,57,58]. In an alkaline environment, CO_2 can not only be directly reduced on the electrode surface but may also react with OH^- ions to form carbonates (CO_3^{2-}) or bicarbonates (HCO_3^-). Specifically, $CO_2 + 2OH^- \rightarrow CO_3^{2-} + H_2O$ and $CO_2 + OH^- \rightarrow HCO_3^-$, both of which cannot directly participate in the reduction reaction, leading to carbon loss and low conversion efficiency [59–61].

To address the above issue, acidic electrolytes have become an emerging area of interest in CO_2RR, effectively avoiding the CO_3^{2-} and HCO_3^-, while a higher H^+ concentration makes HER more kinetically favorable. To suppress HER, researchers have proposed various strategies. For example, Bondue et al. [62] studied CO_2RR on gold electrodes under mild acidic conditions and found that the rates of CO and OH^- generation must be sufficiently high to effectively suppress HER. Huang et al. [24] reported that adding high concentrations of alkaline metal cations (AMCs) to acidic electrolytes can enhance the local pH or electric field, effectively increasing the current density. Additionally, active site engineering has been applied to adjust the interaction between key intermediates like *COOH, *OCOH, and *OCCO with the catalyst surface. However, the stability of CO_2RR in

acidic electrolytes is much lower than that in basic ones, as the higher H^+ concentration and the lack of HCO_3^-/CO_3^{2-} ions hinder stable progression. Meanwhile, the acidic environment leads to the dissolution of many metal or metal oxide catalysts, and the degradation is uncontrollable [63–67].

Apart from bulk pH, the local pH at the EEI significantly affects catalytic selectivity and product distribution. Hori et al. [68] were the first to propose that local pH could alter the reaction pathways of CO_2RR. The local pH is related to the formation of key intermediates, primarily because it can determine proton transfer or rate-limiting steps (RLSs), as shown in Figure 3. Specifically, H^+ can couple to generate H_2 or undergo PCET with the *CO to generate *CHO (a key reaction step for CH_4). In contrast, for multi-carbon products like C_2H_4, the RLS involves C-C coupling, which is less dependent on proton transfer and pH [69]. Notably, increasing the local pH helps reduce the overpotential of C-C coupling at RHE and enhance the selectivity for multi-carbon products [35]. Furthermore, both CH_4 and C_2H_4 formation share the common *CO intermediate, while both CH_4 and H_2 formation involve the common *H, suggesting that the formation of C_1 products is closely related to changes in pH [25,70]. Table 2 compares the FE of various CO_2 reduction products in both alkaline and acidic electrolytes, encompassing both previous and recent advances. The comparative analysis demonstrates that product selectivity depends not only on catalyst composition but is also significantly influenced by key electrolyte parameters, particularly pH and ion effects (cations/anions). These electrolyte-mediated controls have enabled progressive improvements in CO_2 conversion across different reaction pathways.

Table 2. Comparative analysis of electrolyte effects in CO_2RR.

Parameters	Previous Studies	Recent Advances
CO FE	~80% (H_2SO_4 + Cs_2SO_4, Ag) [71]	95% (K_2SO_4, Ag@C) [65] 95% (H_2SO_4, c-PDDA-Ag) [72] 97.1% ($KHCO_3$, Fe_2C-Cs@DC) [73]
HCOOH FE	80% ($KHCO_3$, In NCs) [74] 89.2% (Na_2SO_4, Porous Bi) [75]	90.15% (KOH, BOC/Bi-3) [76] 90.8% (K_2SO_4 + H_2SO_4, Sn-SAC) [77] 93% (K_2SO_4, r-Pb) [77]
CH_4 FE	~57% (KOH, $La_{2-x}CuO_{4-\delta}$) [78]	80% (DMSO, Cu) [79] 71% (H_2SO_4, EDTA-Cu) [80]
C_2H_4 FE	26% (H_3PO_4 + KCl, CAL-Cu) [24] ~63% (KOH, CuO-160W) [81]	70% (K_2SO_4 + H_2SO_4, C/Cu/PTFE) [82] 74% (KOH, Dendritic CuO) [83]

In summary, pH regulates proton availability and the reaction pathways of intermediates, determining the product distribution. Acidic electrolytes help prevent carbonate/bicarbonate formation but may promote HER. Alkaline electrolytes help suppress HER while leading to lower conversion efficiency. At the EEI, local pH changes can influence proton transfer and RLS, which controls the product reaction pathway. Consequently, optimizing pH can effectively enhance CO_2RR efficiency, especially for multi-carbon products.

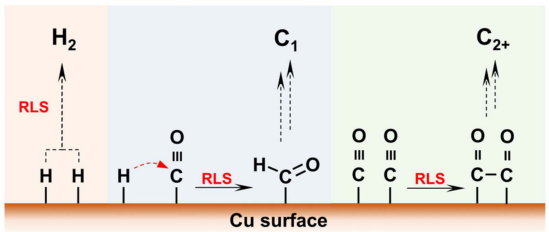

Figure 3. The mechanism model for C_1, C_{2+} and H_2 evolution [35]. Copyright 2022, American Chemical Society.

4. Cation Effects

Cations in the electrolyte are considered to be critical factors influencing the kinetics and product selectivity of electrocatalytic CO_2RR, and their interactions with the electrode include specific adsorption and electrostatic adsorption (long-range interactions) [84,85]. According to the classical theory of the EDL, particularly the Gouy–Chapman–Stern (GCS) model [86,87], the specifically adsorbed species reside at the inner Helmholtz plane (IHP), while the electrostatically adsorbed species are located at the outer Helmholtz plane (OHP), as illustrated in Figure 4a. In the GCS model, there is no potential gradient along the planes parallel to the electrode surface, and the potential only varies in the direction perpendicular to the electrode surface. Murata et al. [88] first demonstrated that the activity and selectivity of CO_2RR are influenced by AMCs, such as Li^+, Na^+, K^+, Cs^+, in the electrolyte on Cu catalysts. Based on the EDL structure, the larger the size of the AMCs ($Li^+ < Na^+ < K^+ < Cs^+$), the smaller the degree of hydration, with the hydration thickness following the order $Cs^+ + nH_2O < K^+ + nH_2O < Na^+ + nH_2O < Li^+ + nH_2O$ [89], as shown in Figure 4b. Hydrated cations are generally adsorbed at the OHP rather than directly on the electrode surface, with their hydration shells interacting with the negative charges on the cathode [90–92]. Although various studies have been conducted on cations and proposed thorites to elucidate these effects, the cations mechanisms remain multifaceted. Typically, the role of cations in CO_2RR can be categorized into three aspects: (1) modulating the interfacial electric field through non-covalent interactions; (2) controlling local CO_2 concentration by buffering the interfacial pH; and (3) stabilizing intermediates through electric field–dipole interactions [92–94].

Non-covalent interactions, such as electrostatic interactions, lead cations to accumulate at the OHP, thereby altering the activity and selectivity of CO_2RR [95]. The strength of the interfacial electric field (IEF) is the primary reason for the gradual increase in CO_2RR reactivity from Li^+ to Cs^+ [96]. Figure 4c illustrates that, at −0.7 V, when the cation in the electrolyte is replaced from Li^+ to Cs^+, the current densities of C_{2+} and H_2 significantly increase, while CH_4 becomes a minor product for all cations. The trend of CO_2RR reactivity in the presence of different AMCs is generally consistent with that in HCO_3^- electrolytes reported by Resasco [93]. DFT calculations also confirm the value of the electrostatic stabilization. As shown in Figure 4d, during the electrochemical reduction of CO on Cu (100), the size of the AMCs affects the local current at the same potential. Similarly, the partial currents of $HCOO^-$, C_2H_4, and C_2H_5OH generated on the Cu (111) surface also increase with the size of the cation. Nevertheless, Resasco suggest that the generation rates of H_2 and CH_4 are less influenced by cation size, which may be due to the absence of a dipole in the hydrogen ion or the presence of distinct counter-ions in the electrolyte (e.g., OH^- and HCO_3^-). Additionally, AMCs adsorbed at the OHP can suppress HER by altering the distribution of the IEF, limiting the migration of hydrated hydrogen ions to the cathode surface [97]. In comparison, the electric field of cations is more likely to stabilize CO rather than *CHO (the intermediate of CH_4), which affects the formation of C_1 products [93]. These trends are consistent with previous studies [92,98]. Hydrated cations with smaller sizes have larger surface charges and interfacial fields, thus requiring a smaller driving force for CO_2RR at specific potentials. Therefore, cations are considered a necessary condition for promoting the CO_2RR reaction.

Another theory posits that hydrated AMCs undergo hydrolysis reactions, acting as buffering agents to regulate the local pH and CO_2 concentration at the EEI [92]. The O–H bonds within the hydration shells exhibit enhanced polarization through interactions with the negatively charged cathode, thereby facilitating the adsorption performance. This phenomenon shifts the OHP potential more negative, and increases the hydrogen ion concentration at the EEI and lower the local pH. In contrast to HER, a low-pH environment

favors CO_2RR, as the efficiency of CO_2RR can be enhanced under elevated CO_2 concentrations compared to HER, which is predominantly affected by a low pH [92]. Ayemoba et al. [99] and Zhang [100] independently determined the local pH of different AMCs during CO_2RR using in-site surface-enhanced infrared absorption spectroscopy (SEIRAS) and rotating ring-disk electrode (RRDE) techniques, respectively. The results propose that the local pH follows the trend $Li^+ > Na^+ > K^+ > Cs^+$ (Figure 4e), consistent with conclusions of Murata [88]. However, direct experimental validation of the interfacial CO_2 concentration trends under varying cations in CO_2RR conditions remains lacking [101]. Contrary to the cation-buffering hypothesis, Malkani et al. [101] employed SEIRAS to probe the interfacial CO_2 concentration dependence on cation size for a Au electrode under −0.8 V, revealing that larger AMCs correlate with lower interfacial CO_2 concentrations (Figure 4f). Although the cation hydrolysis theory was developed based on Ag and Cu surfaces, which differ from Au in their potential of zero charge, the cation-buffering effect on interfacial CO_2 concentration exhibits similar trends across Au, Ag, and Cu surfaces [99]. This study, combining reaction activity and spectroscopic results, demonstrates that interfacial CO_2 concentration is primarily governed by reaction kinetics rather than cation-buffering capacity.

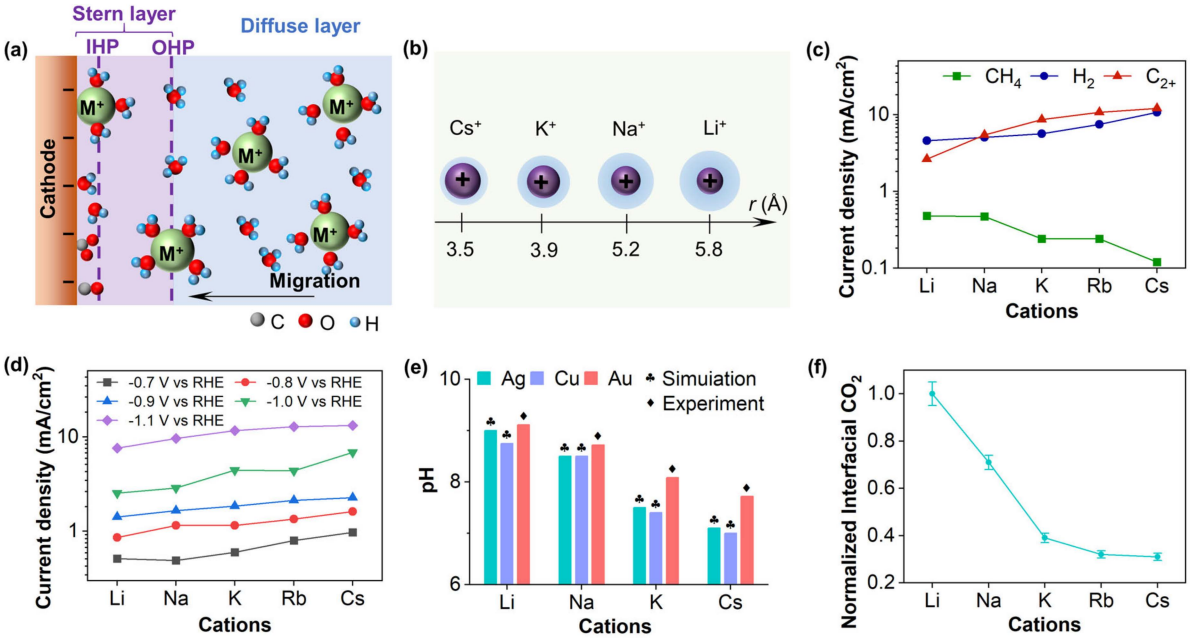

Figure 4. (**a**) Schematic diagram of the electric double layer. (**b**) The radius of the hydrated alkali metal cation [89]. (**c**) Current density on carbon paper supported Cu microparticles at −0.7 V [96]. Copyright 2020, American Association for the Advancement of Science. (**d**) Average current densities obtained during bulk electrolysis on Cu (100) as a function of metal cation at different potentials [93]. (**e**) Steady-state pH at different metal−electrolyte interfaces at −1 V vs. RHE [99]. (**f**) Tracking the interfacial CO_2 concentration for the different alkali metal bicarbonate electrolytes by normalizing to the band area with Li [101]. All figures (**b**,**d**–**f**) are adapted from the American Chemical Society, Copyright 2017–2024.

In the third theoretical framework, cations can influence CO_2RR by inducing interactions between the electric field within the EDL and intermediates with large dipole moments, such as $*CO_2$, *CO, and *OCCO. Specifically adsorbed AMCs at the electrode surface significantly modulate the binding strength or coverage of these intermediates [24,85]. Resasco et al. [93] propose that pronounced dipole interactions exist between adsorbed intermediates and hydrated cations, with interaction strengths following the order $Cs^+ > Rb^+ > K^+ > Na^+ > Li^+$. According to density functional theory (DFT) calculations, this trend arises from the higher concentration of larger cations at the OHP. Further studies

corroborate this theory; for instance, Ovalle et al. [102] utilized SEIRAS to investigate the displacement effects of tetramethylammonium (Me_4N^+) against AMCs, revealing an adsorption sequence of $Li^+ < Na^+ < K^+ < Cs^+$. Additionally, Monteiro et al. [103] demonstrated that CO_2 cannot be reduced to CO on Au, Ag, or Cu electrodes in the absence of AMCs, thereby ruling out the influence of cation-mediated electric fields and pH buffering on CO_2RR. Based on these studies, the authors propose three cation effects: (1) stabilizing intermediates via short- and medium-range interactions; (2) activating CO_2 by reducing the O–C–O bond angle; and (3) enhancing electron transfer rates from the electrode surface to CO_2. Furthermore, Monteiro et al. [31] explored the impact of cations with varying valences (e.g., Cs^+, Ba^{2+}, Nd^{3+}) on CO_2RR the HER. They argue that +3-valent cations have stronger acidity and higher hydrolysis propensity and can promote HER. Specifically, strongly acidic Nd^{3+} facilitates hydrolysis, leading to water reduction even at low overpotentials. In contrast, Cs^+ and Ba^{2+} exhibit slower hydrolysis kinetics, thereby favoring CO_2RR.

In summary, cation size significantly impacts CO_2RR performance, with larger AMCs generally enhancing C_{2+} production while suppressing CH_4. This occurs through three key mechanisms: (1) stronger interfacial electric fields that stabilize *CO intermediates, (2) local pH buffering that increases CO_2 concentration, and (3) dipole interactions with key intermediates. Faradaic efficiency for C_{2+} products improves with cation size (up to ~60% for Cs^+), while current densities increase due to enhanced electric fields. However, trivalent cations (e.g., Nd^{3+}) favor HER through acidic hydrolysis. These effects collectively demonstrate how cation selection can tune product selectivity.

5. Anion Effects

Anions, as an indispensable component of the electrolyte, are also crucial for CO_2RR. Current research primarily focuses on specifically adsorbed anions, which chemically interact with the electrode substrate or undergo chemisorption with other electrolyte species. This interaction can dramatically alter reaction rates and selectivity by modulating the local pH at the EEI via buffering capacity, restructuring the catalyst surface, and affecting the adsorption/desorption of intermediates [85,104]. In the electrocatalytic process, anions are able to occupy active sites, leading to catalyst poisoning and hindering the adsorption of reactants or intermediates, thereby slowing down reaction kinetics [33]. Contrary to this conclusion, some studies have proposed that certain anions can enhance reaction kinetics, and the coverage of adsorbed anions should not be excessive [34,105].

The protons transfer near the electrode generates a large amount of OH^-. Acting as a proton donor, phosphate ions ($H_2PO_4^-$) can neutralize OH^- to buffer the interfacial pH to maintain a low value [106,107]. In contrast, anions such as perchlorate (ClO_4^-), sulfate (SO_4^{2-}), and halides (e.g., Cl^-, Br^-, I^-) may elevate the local pH due to the lack of effective neutralizing species, which inhibits the formation of certain products [108–112]. Dunwell et al. [59] proposed that most CO_2(aq) in the electrolyte originates from the equilibrium with HCO_3^- rather than the diffusion of CO_2(g). In other words, HCO_3^- serves as a carbon source to promote CO generation on Au electrodes, although it does not directly participate in the RLS of the CO formation [113]. Instead, it acts as a proton donor for both CO_2RR and HER in the electrolyte, as shown in Figure 5a, complicating the role of HCO_3^-. Previous studies have compared the buffering effects of several anions on local pH using pKa (Figure 5b), revealing the following order of pH increase: $H_2PO_4^- < HCO_3^- < ClO_4^-$. Although ClO_4^- can suppress HER, the slower kinetics result in a lower selectivity at higher potentials [114]. As a supplement, the buffering capacity of $KHCO_3$, KCl and phosphate electrolytes on the CO_2RR rate and local pH were explored [106]. Under CO_2-limiting conditions, the CO_2 consumption rate (J_{lim}) in $KHCO_3$ solutions is notably higher than that in KCl solutions (Figure 5c). Specifically, at higher CO_2 pressures (P_{CO_2}), $_{lim}$ exhibits

nearly linear growth in KCl solutions, whereas it exhibits a nonlinear increase in $KHCO_3$ solutions. Consequently, the CO_2RR is not only influenced by $KHCO_3$ concentration but is also closely related to its excellent buffering capacity. The simulation results in Figure 5d further demonstrate that $KHCO_3$ can maintain a relatively stable pH at the EEI, preventing excessive alkalinity in the local environment. On the contrary, KCl electrolytes lack buffering capacity, causing a pronounced pH increase at the electrode surface.

Halide ions (e.g., Br^-, I^-, Cl^-) can promote CO_2RR, especially on Cu electrodes. On Cu (100) surfaces, halide ions enhance the FE of C_2 products while reducing H_2 [111]. At −1.23 V, the FE of C_2H_4 in KI electrolyte reaches 50.3%, which is higher than the 30.6% observed in the $KClO_4$ electrolyte. Similarly, the FE of C_2H_5OH increases from 7.1% to 16.4%, while that of CO rises from 11.8% to 22.8%. These results indicate that I^- can alter the electronic environment of *CO, enhancing its adsorption strength and surface coverage, and effectively lowering the energy barrier for C–C coupling. Also, halide ions are crucial in restructuring the catalyst surface, leading to the formation of highly rough surfaces that provide more active sites [34]. For instance, Garg et al. [115] investigated the effects of different halide ions in choline-based electrolytes on reducing CO_2 to CO on the Ag electrode. They illustrated that the FE of CO follows the order $Cl^- > Br^- > I^-$. At more negative potentials, halide ions promote the dissolution and redeposition of Ag electrodes, forming high-index crystal facets, such as (220), (311) (222). Beyond restructuring catalyst surface, halide ions also modulate the formation of key intermediates in the reaction pathway. Their charge-enabling properties facilitate the formation of *COOH, not only reducing the overpotential but also increasing the number of adsorbed CO species available for coupling [111,116]. Wang et al. [4] studied the effects of three different anions (F^-, Cl^-, HCO_3^-) on CO_2RR and proposed an anion enrichment strategy to regulate ion adsorption and desorption. By periodically applying positive potentials to the cathode during pulsed electrolysis, anions can be adsorbed in the IHP, increasing the local anion concentration (Figure 5f). The results show that KF, KCl, and $KHCO_3$ electrolytes exhibit the highest selectivity for CO, C_{2+} and CH_4, respectively, as illustrated in Figure 5e. The strong electronegativity of F^- enables it to strongly adsorb on the electrode surface, inhibiting further reduction of *CO. The moderate adsorption strength of Cl^- favors C–C coupling between *CO species. For HCO_3^-, its strong proton-donating ability promotes the hydrogenation of *CO, enhancing CH_4 selectivity. A key advantage of this strategy is that pulsed electrolysis periodically pushes protons away from the electrode surface, reducing the proton source and significantly suppressing HER.

Organic anions primarily influence CO_2RR by restructuring the electrode surface. For instance, under −0.8 V vs. RHE, propionate ($C_3H_5CO_2^-$) increases the FE of CO to 98.7%, far exceeding the 80% achieved with HCO_3^- [114]. Molecular dynamics simulations reveal that carboxylate form a suitable interfacial water structure through weak adsorption on the electrode surface, promoting CO_2 reduction while inhibiting HER. Additionally, Ge et al. [110] investigated the effects of different anionic surfactants, including sodium dodecylbenzene sulfonate (SDS), sodium lauryl sulfate (SLS), sodium monolauryl phosphate (SMP), and sodium laurate (SL), in $KHCO_3$ electrolyte. They found that these additives significantly improved the FE of CO at −1.2 V vs. RHE, reaching 89.7%, 97.5%, 98.4%, and 98.9%, respectively, far exceeding the 53.1% FE observed in the absence of surfactants. Simultaneously, the FE of H_2 significantly decreased. These results demonstrate that surfactants not only enhance CO selectivity but also suppress HER. In-site attenuated total reflection surface-enhanced infrared spectroscopy (ATR-SEIRAS) analysis revealed that surfactants strengthen the H-bond network of interfacial water molecules, promoting proton-coupled reactions and inhibiting HER. DFT calculations further support these anions in improving water structure, showing that SL and SMP exhibit a stronger H-bond than

SDS and SLS. The organic compound dodecyl phosphate (DDPA) also can restructure the H-bond network at the EEI, increasing the proportion of free water [117]. DDPA increases the FE of CO from 70% to 98% at −1.0 V vs. RHE, maintaining over 90% efficiency for 8 h in flow electrolysis, demonstrating a significant enhancement in CO_2 reduction performance.

In summary, anions have remarkable effects on CO_2RR performance through multiple mechanisms: (1) pH regulation via buffering capacity (e.g., $H_2PO_4^-$ maintains a low pH while ClO_4^- elevates it), (2) surface restructuring (halides create rough surfaces and high-index facets), and (3) intermediate stabilization (I^- enhances *CO adsorption for C–C coupling). These effects lead to distinct product distributions—halides boost C_2+ Faradaic efficiency, while F^- favors CO and HCO_3^- promotes CH_4. Organic anions like carboxylates and surfactants further enhance CO selectivity (up to 98.9% FE) by optimizing interfacial water structure. Current density variations arise from altered reaction kinetics, with buffering anions sustaining higher CO_2 consumption rates than non-buffering ones. The interplay between anion-specific adsorption strength and proton management ultimately dictates reaction pathway length, with moderately adsorbing species favoring multi-carbon products while strongly adsorbing ones that terminate at CO.

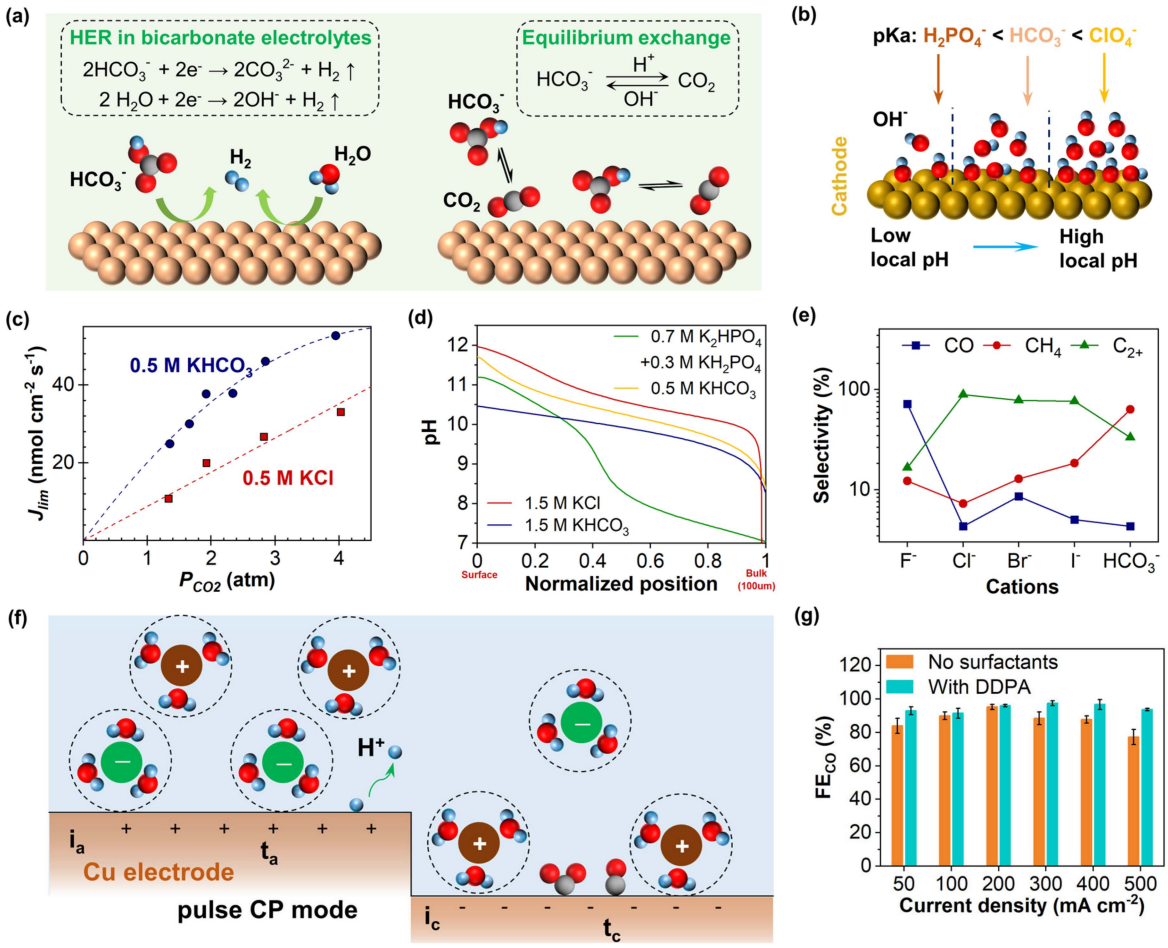

Figure 5. (**a**) Schematic diagram of the equilibrium conversion mechanism between CO_2 and bicarbonate, and (**b**) the effect of the buffering capacity of anions on local pH [85]. Copyright 2024, John Wiley and Sons Ltd. (**c**) CO_2 pressure (P_{CO_2}) dependence of the limiting rate of mass transport of CO_2 ($_{lim}$) in 0.5 M $KHCO_3$ and 0.5 M KCl solutions, and (**d**) pH within the 100 µm boundary layer at P_{CO_2} of 2 atm [106]. (**e**) The selectivity of CO, CH_4, and C_2 as a function of anions, and (**f**) schematic illustrations for the structures of an electric double layer under pulsed CP mode [4]. (**g**) FE of CO at different potentials [117]. Copyright 2018, 2023, and 2024. American Chemical Society.

6. Summary and Outlook

This review summarizes the critical role of the electrolyte in electrochemical CO_2RR, including the effects of pH, cations, and anions on reaction pathways, activity, and selectivity. The research shows the following findings:

1. The configuration of reaction intermediates significantly influences the product formation, and exploring the universality of pathways remains a key focus.
2. The local pH of the electrolyte not only affects the source of protons but also regulates intermediates.
3. Cations significantly affect the kinetics and selectivity of CO_2RR through non-covalent interactions, buffering the interface pH, and stabilizing intermediates.
4. Anions alter the reaction rate and product distribution by regulating local pH, catalyst surface reconstruction, and the adsorption/desorption processes of intermediates.

Although numerous studies have highlighted the critical role of the electrolyte environment in CO_2RR, several key challenges and unresolved questions remain. Addressing these challenges will be essential for advancing the field and improving the efficiency and selectivity of CO_2RR.

1. The interaction mechanisms between the effects of cations and anions are not yet fully understood, particularly in complex electrolyte systems, making it difficult to isolate and analyze individual contributions.
2. The stability of CO_2RR in acidic electrolytes remains a significant issue, as catalyst dissolution and dynamic changes in the local microenvironment require further investigation.
3. The formation pathways of multi-carbon products are intricate, necessitating a combination of advanced experimental techniques and theoretical calculations to elucidate the underlying reaction mechanisms.

Author Contributions: Conceptualization, J.Z. (Jiandong Zhang) and Z.Z.; methodology, J.Z. (Jiandong Zhang) and Z.Z.; investigation, J.Z. (Jiandong Zhang), Z.Z., T.C., J.Z. (Jiayi Zhang) and Y.Z.; writing—original draft preparation, J.Z. (Jiandong Zhang) and Z.Z.; writing—review and editing, J.Z. (Jiandong Zhang), Z.Z., T.C., J.Z. (Jiayi Zhang) and Y.Z., J.Z. (Jiandong Zhang) and Z.Z. are co-first authors. J.Z. (Jiandong Zhang) played a leading role in the literature review and paper writing. Z.Z. provided important support in the data analysis and chart production. All authors have read and agreed to the published version of the manuscript.

Funding: This research was partly supported by the Student Innovation and Entrepreneurship Training Program of China (Project Nos.xj2024118450017).

Data Availability Statement: The data that support the findings of this study are available from the corresponding authors upon reasonable request.

Conflicts of Interest: The authors declare that the research was conducted in the absence of any commercial or financial relationships that could be construed as a potential conflict of interest.

References

1. DuanMu, J.-W.; Gao, F.-Y.; Gao, M.-R. A Critical Review of Operating Stability Issues in Electrochemical CO_2 Reduction. *Sci. China Mater.* **2024**, *67*, 1721–1739. [CrossRef]
2. Zhu, Y.-Z.; Wang, K.; Zheng, S.-S.; Wang, H.-J.; Dong, J.-C.; Li, J.-F. Application and development of electrochemical spectroscopy methods. *Acta Phys.-Chim. Sin.* **2024**, *40*, 2304040. [CrossRef]
3. Chen, Y.; Chen, C.; Cao, X.; Wang, Z.; Zhang, N.; Liu, T. Recent Advances in Defect and Interface Engineering for Electroreduction of CO_2 and N_2. *Acta Phys. Chim. Sin.* **2023**, *39*, 2210053. [CrossRef]
4. Wang, J.; Qin, Y.; Jin, S.; Yang, Y.; Zhu, J.; Li, X.; Lv, X.; Fu, J.; Hong, Z.; Su, Y.; et al. Customizing CO_2 Electroreduction by Pulse-Induced Anion Enrichment. *J. Am. Chem. Soc.* **2023**, *145*, 26213–26221. [CrossRef]

5. Chen, S.; Liu, J.; Zhang, Q.; Teng, F.; McLellan, B.C. A Critical Review on Deployment Planning and Risk Analysis of Carbon Capture, Utilization, and Storage (CCUS) toward Carbon Neutrality. *Renew. Sustain. Energy Rev.* **2022**, *167*, 112537. [CrossRef]
6. Dutta, N.; Bagchi, D.; Chawla, G.; Peter, S.C. A Guideline to Determine Faradaic Efficiency in Electrochemical CO_2 Reduction. *ACS Energy Lett.* **2024**, *9*, 323–328. [CrossRef]
7. Jiao, J.; Kang, X.; Yang, J.; Jia, S.; Chen, X.; Peng, Y.; Chen, C.; Xing, X.; Chen, Z.; He, M.; et al. Lattice Strain Engineering Boosts CO_2 Electroreduction to C_{2+} Products. *Angew. Chem. Int. Ed.* **2024**, *63*, e202409563. [CrossRef]
8. Li, H.; Jiang, Y.; Li, X.; Davey, K.; Zheng, Y.; Jiao, Y.; Qiao, S.-Z. C_{2+} Selectivity for CO_2 Electroreduction on Oxidized Cu-Based Catalysts. *J. Am. Chem. Soc.* **2023**, *145*, 14335–14344. [CrossRef]
9. Ma, L.; Zhao, W.; Wang, B.; Ling, L.; Zhang, R. CO_2 Activation and Conversion on Cu Catalysts: Revealing the Role of Cu Surface Defect Types in Tuning the Activity and Selectivity. *Fuel* **2022**, *313*, 122686. [CrossRef]
10. Song, X.; Xiong, W.; He, H.; Si, D.; Lü, L.; Peng, Y.; Jiang, Q.; Wang, Y.; Zheng, Y.; Nan, Z.-A.; et al. Boosting CO_2 Electrocatalytic Reduction to Ethylene via Hydrogen-Assisted C-C Coupling on Cu_2O Catalysts Modified with Pd Nanoparticles. *Nano Energy* **2024**, *122*, 109275. [CrossRef]
11. Zhu, W.; Liu, S.; Zhao, K.; Su, Y.; Yang, Y.; Huang, K.; He, Z. Activating *CO by Strengthening Fe–CO Π-backbonding to Enhance Two-carbon Products Formation toward CO_2 Electroreduction on Fe–N_4 Sites. *Adv. Funct. Mater.* **2024**, *34*, 2402537. [CrossRef]
12. Su, S.; Zhou, Y.; Xiong, L.; Jin, S.; Du, Y.; Zhu, M. Structure-activity Relationships of the Structural Analogs Au_8Cu_1 and Au_8Ag_1 in the Electrocatalytic CO_2 Reduction Reaction. *Angew. Chem. Int. Ed.* **2024**, *136*, e202404629. [CrossRef]
13. Li, Y.; Wei, Z.; Sun, Z.; Zhai, H.; Li, S.; Chen, W. Sulfur Modified Carbon-based Single-atom Catalysts for Electrocatalytic Reactions. *Small* **2024**, *20*, 2401900. [CrossRef]
14. Yuan, F.; Wang, X.; Ma, T.; Fan, J.; Lai, X.; Liu, Y. Enhanced Conversion of CO_2 into C_2H_4 on Single Atom Cu-Anchored Graphitic Carbon Nitride: Synergistic Diatomic Active Sites Interaction. *J. Colloid Interface Sci.* **2024**, *667*, 291–302. [CrossRef] [PubMed]
15. Hung, S.-F.; Xu, A.; Wang, X.; Li, F.; Hsu, S.-H.; Li, Y.; Wicks, J.; Cervantes, E.G.; Rasouli, A.S.; Li, Y.C.; et al. A Metal-Supported Single-Atom Catalytic Site Enables Carbon Dioxide Hydrogenation. *Nat. Commun.* **2022**, *13*, 819. [CrossRef] [PubMed]
16. Yang, H.; Li, S.; Xu, Q. Efficient Strategies for Promoting the Electrochemical Reduction of CO_2 to C_2+ Products over Cu-Based Catalysts. *Chin. J. Catal.* **2023**, *48*, 32–65. [CrossRef]
17. Liu, C.; Gong, J.; Gao, Z.; Xiao, L.; Wang, G.; Lu, J.; Zhuang, L. Regulation of the Activity, Selectivity, and Durability of Cu-Based Electrocatalysts for CO_2 Reduction. *Sci. China Chem.* **2021**, *64*, 1660–1678. [CrossRef]
18. Nitopi, S.; Bertheussen, E.; Scott, S.B.; Liu, X.; Engstfeld, A.K.; Horch, S.; Seger, B.; Stephens, I.E.L.; Chan, K.; Hahn, C.; et al. Progress and Perspectives of Electrochemical CO_2 Reduction on Copper in Aqueous Electrolyte. *Chem. Rev.* **2019**, *119*, 7610–7672. [CrossRef]
19. Chu, M.; Chen, C.; Wu, Y.; Yan, X.; Jia, S.; Feng, R.; Wu, H.; He, M.; Han, B. Enhanced CO_2 Electroreduction to Ethylene via Strong Metal-Support Interaction. *Green Energy Environ.* **2022**, *7*, 792–798. [CrossRef]
20. Liu, Y.; Song, Y.; Huang, L.; Su, J.; Li, G.; Zhang, Q.; Xin, Y.; Cao, X.; Guo, W.; Dou, Y.; et al. Constructing Ionic Interfaces for Stable Electrochemical CO_2 Reduction. *ACS Nano* **2024**, *18*, 14020–14028. [CrossRef]
21. Hou, J.; Xu, B.; Lu, Q. Influence of Electric Double Layer Rigidity on CO Adsorption and Electroreduction Rate. *Nat. Commun.* **2024**, *15*, 1926. [CrossRef]
22. Gebbie, M.A.; Liu, B.; Guo, W.; Anderson, S.R.; Johnstone, S.G. Linking Electric Double Layer Formation to Electrocatalytic Activity. *ACS Catal.* **2023**, *13*, 16222–16239. [CrossRef]
23. Xu, A.; Govindarajan, N.; Kastlunger, G.; Vijay, S.; Chan, K. Theories for Electrolyte Effects in CO_2 Electroreduction. *Acc. Chem. Res.* **2022**, *55*, 495–503. [CrossRef] [PubMed]
24. Huang, J.E.; Li, F.; Ozden, A.; Sedighian Rasouli, A.; García De Arquer, F.P.; Liu, S.; Zhang, S.; Luo, M.; Wang, X.; Lum, Y.; et al. CO_2 Electrolysis to Multicarbon Products in Strong Acid. *Science* **2021**, *372*, 1074–1078. [CrossRef]
25. Schreier, M.; Yoon, Y.; Jackson, M.N.; Surendranath, Y. Competition between H and CO for Active Sites Governs Copper-mediated Electrosynthesis of Hydrocarbon Fuels. *Angew. Chem. Int. Ed.* **2018**, *57*, 10221–10225. [CrossRef] [PubMed]
26. Wu, T.; Bu, H.; Tao, S.; Ma, M. Determination of Local pH in CO_2 Electroreduction. *Nanoscale* **2024**, *16*, 3926–3935. [CrossRef] [PubMed]
27. Shin, S.-J.; Choi, H.; Ringe, S.; Won, D.H.; Oh, H.-S.; Kim, D.H.; Lee, T.; Nam, D.-H.; Kim, H.; Choi, C.H. A Unifying Mechanism for Cation Effect Modulating C1 and C2 Productions from CO_2 Electroreduction. *Nat. Commun.* **2022**, *13*, 5482. [CrossRef]
28. Xu, Y.; Xia, Z.; Gao, W.; Xiao, H.; Xu, B. Cation Effect on the Elementary Steps of the Electrochemical CO Reduction Reaction on Cu. *Nat. Catal.* **2024**, *7*, 1120–1129. [CrossRef]
29. Qin, X.; Vegge, T.; Hansen, H.A. Cation-Coordinated Inner-Sphere CO_2 Electroreduction at Au–Water Interfaces. *J. Am. Chem. Soc.* **2023**, *145*, 1897–1905. [CrossRef]
30. Dong, Y.; Ma, M.; Jiao, Z.; Han, S.; Xiong, L.; Deng, Z.; Peng, Y. Effect of Electrolyte Cation-Mediated Mechanism on Electrocatalytic Carbon Dioxide Reduction. *Chin. Chem. Lett.* **2024**, *35*, 109049. [CrossRef]

31. Monteiro, M.C.O.; Dattila, F.; López, N.; Koper, M.T.M. The Role of Cation Acidity on the Competition between Hydrogen Evolution and CO_2 Reduction on Gold Electrodes. *J. Am. Chem. Soc.* **2022**, *144*, 1589–1602. [CrossRef] [PubMed]
32. Hsieh, Y.-C.; Senanayake, S.D.; Zhang, Y.; Xu, W.; Polyansky, D.E. Effect of Chloride Anions on the Synthesis and Enhanced Catalytic Activity of Silver Nanocoral Electrodes for CO_2 Electroreduction. *ACS Catal.* **2015**, *5*, 5349–5356. [CrossRef]
33. Tripkovic, D.V.; Strmcnik, D.; Van Der Vliet, D.; Stamenkovic, V.; Markovic, N.M. The Role of Anions in Surface Electrochemistry. *Faraday Discuss.* **2009**, *140*, 25–40. [CrossRef]
34. Masana, J.J.; Peng, B.; Shuai, Z.; Qiu, M.; Yu, Y. Influence of Halide Ions on the Electrochemical Reduction of Carbon Dioxide over a Copper Surface. *J. Mater. Chem. A* **2022**, *10*, 1086–1104. [CrossRef]
35. Deng, B.; Huang, M.; Zhao, X.; Mou, S.; Dong, F. Interfacial Electrolyte Effects on Electrocatalytic CO_2 Reduction. *ACS Catal.* **2022**, *12*, 331–362. [CrossRef]
36. Lv, J.; Yin, R.; Zhou, L.; Li, J.; Kikas, R.; Xu, T.; Wang, Z.; Jin, H.; Wang, X.; Wang, S. Microenvironment Engineering for the Electrocatalytic CO_2 Reduction Reaction. *Angew. Chem.* **2022**, *134*, e202207252. [CrossRef]
37. Peng, L.; Zhang, Y.; He, R.; Xu, N.; Qiao, J. Research advances in electrocatalysts, electrolytes, reactors and membranes for the electrocatalytic carbon dioxide reduction reaction. *Acta Phys. Chim. Sin.* **2023**, *10*, 2302037. [CrossRef]
38. Chen, B.; Jiang, Y.-F.; Xiao, H.; Li, J. Selective CO_2-to-HCOOH Electroreduction on Graphdiyne-Supported Bimetallic Single-Cluster Catalysts. *ACS Catal.* **2024**, *14*, 10510–10518. [CrossRef]
39. Guan, A.; Chen, Z.; Quan, Y.; Peng, C.; Wang, Z.; Sham, T.-K.; Yang, C.; Ji, Y.; Qian, L.; Xu, X.; et al. Boosting CO_2 Electroreduction to CH_4 via Tuning Neighboring Single-Copper Sites. *ACS Energy Lett.* **2020**, *5*, 1044–1053. [CrossRef]
40. Sebastián-Pascual, P.; Escudero-Escribano, M. Addressing the Interfacial Properties for CO Electroreduction on Cu with Cyclic Voltammetry. *ACS Energy Lett.* **2020**, *5*, 130–135. [CrossRef]
41. Li, S.; Guan, A.; Yang, C.; Peng, C.; Lv, X.; Ji, Y.; Quan, Y.; Wang, Q.; Zhang, L.; Zheng, G. Dual-Atomic Cu Sites for Electrocatalytic CO Reduction to C_{2+} Products. *ACS Mater. Lett.* **2021**, *3*, 1729–1737. [CrossRef]
42. Shi, X.; Shi, L.; Wang, J.; Zhou, Y.; Zhao, S. Defect Engineering of Nanomaterials for Selective Electrocatalytic CO_2 Reduction. *Matter* **2024**, *7*, 4233–4259. [CrossRef]
43. Birdja, Y.Y.; Pérez-Gallent, E.; Figueiredo, M.C.; Göttle, A.J.; Calle-Vallejo, F.; Koper, M.T.M. Advances and Challenges in Understanding the Electrocatalytic Conversion of Carbon Dioxide to Fuels. *Nat. Energy* **2019**, *4*, 732–745. [CrossRef]
44. Dong, J.; Liu, Y.; Pei, J.; Li, H.; Ji, S.; Shi, L.; Zhang, Y.; Li, C.; Tang, C.; Liao, J.; et al. Continuous Electroproduction of Formate via CO_2 Reduction on Local Symmetry-Broken Single-Atom Catalysts. *Nat. Commun.* **2023**, *14*, 6849. [CrossRef] [PubMed]
45. Huang, B.; Wu, Y.; Luo, Y.; Zhou, N. Double Atom-Anchored Defective Boron Nitride Catalyst for Efficient Electroreduction of CO_2 to CH4: A First Principles Study. *Chem. Phys. Lett.* **2020**, *756*, 137852. [CrossRef]
46. Dong, H.; Li, Y.; Jiang, D. First-Principles Insight into Electrocatalytic Reduction of CO_2 to CH_4 on a Copper Nanoparticle. *J. Phys. Chem. C* **2018**, *122*, 11392–11398. [CrossRef]
47. Ali, S.A.; Sadiq, I.; Ahmad, T. Deep Insight of CO_2 Reduction Reaction Mechanism through Experimental and Theoretical Anticipations. *Mater. Today Sustain.* **2023**, *24*, 100587. [CrossRef]
48. Du, P.; Ding, J.; Liu, C.; Li, P.; Liu, W.; Yan, W.; Pan, Y.; Hu, J.; Zhu, J.; Li, X.; et al. Interface-engineering-induced C−C Coupling for C_2H_4 Photosynthesis from Atmospheric-concentration CO_2 Reduction. *Angew. Chem.* **2024**, *137*, e202421353. [CrossRef]
49. Lei, Y.; Wang, Z.; Bao, A.; Tang, X.; Huang, X.; Yi, H.; Zhao, S.; Sun, T.; Wang, J.; Gao, F. Recent Advances on Electrocatalytic CO_2 Reduction to Resources: Target Products, Reaction Pathways and Typical Catalysts. *Chem. Eng. J.* **2023**, *453*, 139663. [CrossRef]
50. Wang, Y.; Chen, E.; Tang, J. Insight on Reaction Pathways of Photocatalytic CO_2 Conversion. *ACS Catal.* **2022**, *12*, 7300–7316. [CrossRef]
51. Zhang, Y.-C.; Zhang, X.-L.; Wu, Z.-Z.; Niu, Z.-Z.; Chi, L.-P.; Gao, F.-Y.; Yang, P.-P.; Wang, Y.-H.; Yu, P.-C.; Duanmu, J.-W.; et al. Facet-Switching of Rate-Determining Step on Copper in CO_2 -to-Ethylene Electroreduction. *Proc. Natl. Acad. Sci. USA* **2024**, *121*, e2400546121. [CrossRef] [PubMed]
52. Qiu, X.-F.; Zhu, H.-L.; Huang, J.-R.; Liao, P.-Q.; Chen, X.-M. Highly Selective CO_2 Electroreduction to C_2H_4 Using a Metal–Organic Framework with Dual Active Sites. *J. Am. Chem. Soc.* **2021**, *143*, 7242–7246. [CrossRef]
53. Meng, D.; Zhang, M.; Si, D.; Mao, M.; Hou, Y.; Huang, Y.; Cao, R. Highly Selective Tandem Electroreduction of CO_2 to Ethylene over Atomically Isolated Nickel–Nitrogen Site/Copper Nanoparticle Catalysts. *Angew. Chem. Int. Ed.* **2021**, *60*, 25485–25492. [CrossRef]
54. Kastlunger, G.; Wang, L.; Govindarajan, N.; Heenen, H.H.; Ringe, S.; Jaramillo, T.; Hahn, C.; Chan, K. Using pH Dependence to Understand Mechanisms in Electrochemical CO Reduction. *ACS Catal.* **2022**, *12*, 4344–4357. [CrossRef]
55. Li, P.; Jiang, Y.; Hu, Y.; Men, Y.; Liu, Y.; Cai, W.; Chen, S. Hydrogen Bond Network Connectivity in the Electric Double Layer Dominates the Kinetic pH Effect in Hydrogen Electrocatalysis on Pt. *Nat. Catal.* **2022**, *5*, 900–911. [CrossRef]
56. Chen, C.; Li, Y.; Yang, P. Address the "Alkalinity Problem" in CO_2 Electrolysis with Catalyst Design and Translation. *Joule* **2021**, *5*, 737–742. [CrossRef]

57. Ooka, H.; Figueiredo, M.C.; Koper, M.T.M. Competition between Hydrogen Evolution and Carbon Dioxide Reduction on Copper Electrodes in Mildly Acidic Media. *Langmuir* **2017**, *33*, 9307–9313. [CrossRef] [PubMed]
58. Grozovski, V.; Vesztergom, S.; Láng, G.G.; Broekmann, P. Electrochemical Hydrogen Evolution: H^+ or H_2 O Reduction? A Rotating Disk Electrode Study. *J. Electrochem. Soc.* **2017**, *164*, E3171–E3178. [CrossRef]
59. Dunwell, M.; Lu, Q.; Heyes, J.M.; Rosen, J.; Chen, J.G.; Yan, Y.; Jiao, F.; Xu, B. The Central Role of Bicarbonate in the Electrochemical Reduction of Carbon Dioxide on Gold. *J. Am. Chem. Soc.* **2017**, *139*, 3774–3783. [CrossRef]
60. Wuttig, A.; Yoon, Y.; Ryu, J.; Surendranath, Y. Bicarbonate Is Not a General Acid in Au-Catalyzed CO_2 Electroreduction. *J. Am. Chem. Soc.* **2017**, *139*, 17109–17113. [CrossRef]
61. Marcandalli, G.; Goyal, A.; Koper, M.T.M. Electrolyte Effects on the Faradaic Efficiency of CO_2 Reduction to CO on a Gold Electrode. *ACS Catal.* **2021**, *11*, 4936–4945. [CrossRef] [PubMed]
62. Bondue, C.J.; Graf, M.; Goyal, A.; Koper, M.T.M. Suppression of Hydrogen Evolution in Acidic Electrolytes by Electrochemical CO_2 Reduction. *J. Am. Chem. Soc.* **2021**, *143*, 279–285. [CrossRef] [PubMed]
63. Shen, H.; Jin, H.; Li, H.; Wang, H.; Duan, J.; Jiao, Y.; Qiao, S.-Z. Acidic CO_2-to-HCOOH Electrolysis with Industrial-Level Current on Phase Engineered Tin Sulfide. *Nat. Commun.* **2023**, *14*, 2843. [CrossRef]
64. Ling, N.; Zhang, J.; Wang, M.; Wang, Z.; Mi, Z.; Bin Dolmanan, S.; Zhang, M.; Wang, B.; Ru Leow, W.; Zhang, J.; et al. Acidic Media Impedes Tandem Catalysis Reaction Pathways in Electrochemical CO_2 Reduction. *Angew. Chem. Int. Ed.* **2023**, *62*, e202308782. [CrossRef] [PubMed]
65. Li, X.; Zhang, P.; Zhang, L.; Zhang, G.; Gao, H.; Pang, Z.; Yu, J.; Pei, C.; Wang, T.; Gong, J. Confinement of an Alkaline Environment for Electrocatalytic CO_2 Reduction in Acidic Electrolytes. *Chem. Sci.* **2023**, *14*, 5602–5607. [CrossRef]
66. Lai, W.; Qiao, Y.; Wang, Y.; Huang, H. Stability Issues in Electrochemical CO_2 Reduction: Recent Advances in Fundamental Understanding and Design Strategies. *Adv. Mater.* **2023**, *35*, 2306288. [CrossRef]
67. Nie, W.; Heim, G.P.; Watkins, N.B.; Agapie, T.; Peters, J.C. Organic Additive-derived Films on Cu Electrodes Promote Electrochemical CO_2 Reduction to C_{2+} Products under Strongly Acidic Conditions. *Angew. Chem. Int. Ed.* **2023**, *62*, e202216102. [CrossRef]
68. Hori, Y.; Murata, A.; Takahashi, R. Formation of Hydrocarbons in the Electrochemical Reduction of Carbon Dioxide at a Copper Electrode in Aqueous Solution. *J. Chem. Soc. Faraday Trans. 1* **1989**, *85*, 2309. [CrossRef]
69. Sargeant, E.; Rodriguez, P.; Calle-Vallejo, F. Cation Effects on the Adsorbed Intermediates of CO_2 Electroreduction Are Systematic and Predictable. *ACS Catal.* **2024**, *14*, 8814–8822. [CrossRef]
70. Raciti, D.; Mao, M.; Wang, C. Mass Transport Modelling for the Electroreduction of CO_2 on Cu Nanowires. *Nanotechnology* **2018**, *29*, 044001. [CrossRef]
71. Pan, B.; Fan, J.; Zhang, J.; Luo, Y.; Shen, C.; Wang, C.; Wang, Y.; Li, Y. Close to 90% Single-Pass Conversion Efficiency for CO_2 Electroreduction in an Acid-Fed Membrane Electrode Assembly. *ACS Energy Lett.* **2022**, *7*, 4224–4231. [CrossRef]
72. Qin, H.-G.; Du, Y.-F.; Bai, Y.-Y.; Li, F.-Z.; Yue, X.; Wang, H.; Peng, J.-Z.; Gu, J. Surface-Immobilized Cross-Linked Cationic Polyelectrolyte Enables CO_2 Reduction with Metal Cation-Free Acidic Electrolyte. *Nat. Commun.* **2023**, *14*, 5640. [CrossRef]
73. Su, J.; Pan, D.; Dong, Y.; Zhang, Y.; Tang, Y.; Sun, J.; Zhang, L.; Tian, Z.; Chen, L. Ultrafine Fe_2 C Iron Carbide Nanoclusters Trapped in Topological Carbon Defects for Efficient Electroreduction of Carbon Dioxide. *Adv. Energy Mater.* **2023**, *13*, 2204391. [CrossRef]
74. Jiang, M.; Zhu, M.; Wang, H.; Song, X.; Liang, J.; Lin, D.; Li, C.; Cui, J.; Li, F.; Zhang, X.L.; et al. Rapid and Green Electric-Explosion Preparation of Spherical Indium Nanocrystals with Abundant Metal Defects for Highly-Selective CO_2 Electroreduction. *Nano Lett.* **2023**, *23*, 291–297. [CrossRef] [PubMed]
75. Yan, T.; Pan, H.; Liu, Z.; Kang, P. Phase-inversion Induced 3D Electrode for Direct Acidic Electroreduction CO_2 to Formic Acid. *Small* **2023**, *19*, 2207650. [CrossRef]
76. Liu, X.; Zheng, H.; Sun, Q.; He, J.; Yao, X.; Sun, C.; Shan, G.; Zhang, M.; Zhu, C.; Su, Z.; et al. Mastering the Lattice Strain in Bismuth-based Electrocatalysts for Efficient CO_2-to-formate Conversion. *Adv. Funct. Mater.* **2024**, *34*, 2400928. [CrossRef]
77. Sun, B.; Li, Z.; Xiao, D.; Liu, H.; Song, K.; Wang, Z.; Liu, Y.; Zheng, Z.; Wang, P.; Dai, Y.; et al. Unveiling pH-dependent Adsorption Strength of $*CO_2^-$ Intermediate over High-density Sn Single Atom Catalyst for Acidic CO_2-to-HCOOH Electroreduction. *Angew. Chem. Int. Ed.* **2024**, *63*, e202318874. [CrossRef] [PubMed]
78. Zhu, J.; Wang, Y.; Zhi, A.; Chen, Z.; Shi, L.; Zhang, Z.; Zhang, Y.; Zhu, Y.; Qiu, X.; Tian, X.; et al. Cation-deficiency-dependent CO_2 Electroreduction over Copper-based Ruddlesden–Popper Perovskite Oxides. *Angew. Chem. Int. Ed.* **2022**, *61*, e202111670. [CrossRef]
79. Kash, B.C.; Gomes, R.J.; Amanchukwu, C.V. Mitigating Electrode Inactivation during CO_2 Electrocatalysis in Aprotic Solvents with Alkali Cations. *J. Phys. Chem. Lett.* **2023**, *14*, 920–926. [CrossRef]
80. Fan, M.; Huang, J.E.; Miao, R.K.; Mao, Y.; Ou, P.; Li, F.; Li, X.-Y.; Cao, Y.; Zhang, Z.; Zhang, J.; et al. Cationic-Group-Functionalized Electrocatalysts Enable Stable Acidic CO_2 Electrolysis. *Nat. Catal.* **2023**, *6*, 763–772. [CrossRef]

81. Zhang, J.; Wang, Y.; Li, Z.; Xia, S.; Cai, R.; Ma, L.; Zhang, T.; Ackley, J.; Yang, S.; Wu, Y.; et al. Grain Boundary-derived Cu^+ /Cu^0 Interfaces in CuO Nanosheets for Low Overpotential Carbon Dioxide Electroreduction to Ethylene. *Adv. Sci.* **2022**, *9*, 2200454. [CrossRef] [PubMed]
82. Wang, Z.; Li, Y.; Zhao, X.; Chen, S.; Nian, Q.; Luo, X.; Fan, J.; Ruan, D.; Xiong, B.-Q.; Ren, X. Localized Alkaline Environment via in Situ Electrostatic Confinement for Enhanced CO_2 -to-Ethylene Conversion in Neutral Medium. *J. Am. Chem. Soc.* **2023**, *145*, 6339–6348. [CrossRef] [PubMed]
83. Yang, R.; Wu, M.; Huang, D.; Yang, Y.; Liu, Y.; Zhang, L.; Lai, F.; You, B.; Fang, J.; Liu, T.; et al. Which Dominates Industrial–Current–Density CO_2 -to-C_{2+} Electroreduction: $Cu^{\delta+}$ or the Microenvironment? *Energy Environ. Sci.* **2024**, *17*, 2897–2907. [CrossRef]
84. Chen, W.; Zhang, L.-L.; Wei, Z.; Zhang, M.-K.; Cai, J.; Chen, Y.-X. The Electrostatic Effect and Its Role in Promoting Electrocatalytic Reactions by Specifically Adsorbed Anions. *Phys. Chem. Chem. Phys.* **2023**, *25*, 8317–8330. [CrossRef]
85. Ma, M.; Seger, B. Rational Design of Local Reaction Environment for Electrocatalytic Conversion of CO_2 into Multicarbon Products. *Angew. Chem. Int. Ed.* **2024**, *63*, e202401185. [CrossRef]
86. Grahame, D.C. The Electrical Double Layer and the Theory of Electrocapillarity. *Chem. Rev.* **1947**, *41*, 441–501. [CrossRef]
87. Devanathan, M.A.V.; Tilak, B.V.K.S.R.A. The Structure of the Electrical Double Layer at the Metal-Solution Interface. *Chem. Rev.* **1965**, *65*, 635–684. [CrossRef]
88. Murata, A.; Hori, Y. Product Selectivity Affected by Cationic Species in Electrochemical Reduction of CO_2 and CO at a Cu Electrode. *Bull. Chem. Soc. Jpn.* **1991**, *64*, 123–127. [CrossRef]
89. Li, Z.; Wang, L.; Sun, L.; Yang, W. Dynamic Cation Enrichment during Pulsed CO_2 Electrolysis and the Cation-Promoted Multicarbon Formation. *J. Am. Chem. Soc.* **2024**, *146*, 23901–23908. [CrossRef]
90. Waegele, M.M.; Gunathunge, C.M.; Li, J.; Li, X. How Cations Affect the Electric Double Layer and the Rates and Selectivity of Electrocatalytic Processes. *J. Chem. Phys.* **2019**, *151*, 160902. [CrossRef]
91. Moura De Salles Pupo, M.; Kortlever, R. Electrolyte Effects on the Electrochemical Reduction of CO_2. *ChemPhysChem* **2019**, *20*, 2926–2935. [CrossRef] [PubMed]
92. Singh, M.R.; Kwon, Y.; Lum, Y.; Ager, J.W.; Bell, A.T. Hydrolysis of Electrolyte Cations Enhances the Electrochemical Reduction of CO_2 over Ag and Cu. *J. Am. Chem. Soc.* **2016**, *138*, 13006–13012. [CrossRef] [PubMed]
93. Resasco, J.; Chen, L.D.; Clark, E.; Tsai, C.; Hahn, C.; Jaramillo, T.F.; Chan, K.; Bell, A.T. Promoter Effects of Alkali Metal Cations on the Electrochemical Reduction of Carbon Dioxide. *J. Am. Chem. Soc.* **2017**, *139*, 11277–11287. [CrossRef]
94. Chen, L.D.; Urushihara, M.; Chan, K.; Nørskov, J.K. Electric Field Effects in Electrochemical CO_2 Reduction. *ACS Catal.* **2016**, *6*, 7133–7139. [CrossRef]
95. Ringe, S.; Clark, E.L.; Resasco, J.; Walton, A.; Seger, B.; Bell, A.T.; Chan, K. Understanding Cation Effects in Electrochemical CO_2 Reduction. *Energy Environ. Sci.* **2019**, *12*, 3001–3014. [CrossRef]
96. Malkani, A.S.; Li, J.; Oliveira, N.J.; He, M.; Chang, X.; Xu, B.; Lu, Q. Understanding the Electric and Nonelectric Field Components of the Cation Effect on the Electrochemical CO Reduction Reaction. *Sci. Adv.* **2020**, *6*, eabd2569. [CrossRef] [PubMed]
97. Gu, J.; Liu, S.; Ni, W.; Ren, W.; Haussener, S.; Hu, X. Modulating Electric Field Distribution by Alkali Cations for CO_2 Electroreduction in Strongly Acidic Medium. *Nat. Catal.* **2022**, *5*, 268–276. [CrossRef]
98. Thorson, M.R.; Siil, K.I.; Kenis, P.J.A. Effect of Cations on the Electrochemical Conversion of CO_2 to CO. *J. Electrochem. Soc.* **2013**, *160*, F69–F74. [CrossRef]
99. Ayemoba, O.; Cuesta, A. Spectroscopic Evidence of Size-Dependent Buffering of Interfacial pH by Cation Hydrolysis during CO_2 Electroreduction. *ACS Appl. Mater. Interfaces* **2017**, *9*, 27377–27382. [CrossRef]
100. Zhang, Z.-M.; Wang, T.; Cai, Y.-C.; Li, X.-Y.; Ye, J.-Y.; Zhou, Y.; Tian, N.; Zhou, Z.-Y.; Sun, S.-G. Probing Electrolyte Effects on Cation-Enhanced CO_2 Reduction on Copper in Acidic Media. *Nat. Catal.* **2024**, *7*, 807–817. [CrossRef]
101. Malkani, A.S.; Anibal, J.; Xu, B. Cation Effect on Interfacial CO_2 Concentration in the Electrochemical CO_2 Reduction Reaction. *ACS Catal.* **2020**, *10*, 14871–14876. [CrossRef]
102. Ovalle, V.J.; Hsu, Y.-S.; Agrawal, N.; Janik, M.J.; Waegele, M.M. Correlating Hydration Free Energy and Specific Adsorption of Alkali Metal Cations during CO_2 Electroreduction on Au. *Nat. Catal.* **2022**, *5*, 624–632. [CrossRef]
103. Monteiro, M.C.O.; Dattila, F.; Hagedoorn, B.; García-Muelas, R.; López, N.; Koper, M.T.M. Absence of CO_2 Electroreduction on Copper, Gold and Silver Electrodes without Metal Cations in Solution. *Nat. Catal.* **2021**, *4*, 654–662. [CrossRef]
104. Chen, W.; Du, X.; Tao, S.; Lin, B.; Tranca, I.; Tielens, F.; Ma, M.; Liu, Z. Electrolyte Effects on Reaction Kinetics in Electrochemical CO_2 Reduction: The Roles of pH, Cations, and Anions. *Chem. Phys. Rev.* **2025**, *6*, 011302. [CrossRef]
105. Gao, D.; Sinev, I.; Scholten, F.; Arán-Ais, R.M.; Divins, N.J.; Kvashnina, K.; Timoshenko, J.; Roldan Cuenya, B. Selective CO_2 Electroreduction to Ethylene and Multicarbon Alcohols via Electrolyte-driven Nanostructuring. *Angew. Chem. Int. Ed.* **2019**, *58*, 17047–17053. [CrossRef]

106. Hashiba, H.; Weng, L.-C.; Chen, Y.; Sato, H.K.; Yotsuhashi, S.; Xiang, C.; Weber, A.Z. Effects of Electrolyte Buffer Capacity on Surface Reactant Species and the Reaction Rate of CO_2 in Electrochemical CO_2 Reduction. *J. Phys. Chem. C* **2018**, *122*, 3719–3726. [CrossRef]
107. Resasco, J.; Lum, Y.; Clark, E.; Zeledon, J.Z.; Bell, A.T. Effects of Anion Identity and Concentration on Electrochemical Reduction of CO_2. *ChemElectroChem* **2018**, *5*, 1064–1072. [CrossRef]
108. Tomisaki, M.; Kasahara, S.; Natsui, K.; Ikemiya, N.; Einaga, Y. Switchable Product Selectivity in the Electrochemical Reduction of Carbon Dioxide Using Boron-Doped Diamond Electrodes. *J. Am. Chem. Soc.* **2019**, *141*, 7414–7420. [CrossRef]
109. Moradzaman, M.; Mul, G. Optimizing CO Coverage on Rough Copper Electrodes: Effect of the Partial Pressure of CO and Electrolyte Anions (pH) on Selectivity toward Ethylene. *J. Phys. Chem. C* **2021**, *125*, 6546–6554. [CrossRef]
110. Ge, W.; Zhu, Y.; Wang, H.; Jiang, H.; Li, C. Anionic Surfactant-Tuned Interfacial Water Reactivity Promoting Electrocatalytic CO_2 Reduction. *ACS Catal.* **2024**, *14*, 18156–18166. [CrossRef]
111. Huang, Y.; Ong, C.W.; Yeo, B.S. Effects of Electrolyte Anions on the Reduction of Carbon Dioxide to Ethylene and Ethanol on Copper (100) and (111) Surfaces. *ChemSusChem* **2018**, *11*, 3299–3306. [CrossRef] [PubMed]
112. Gao, D.; Arán-Ais, R.M.; Jeon, H.S.; Roldan Cuenya, B. Rational Catalyst and Electrolyte Design for CO_2 Electroreduction towards Multicarbon Products. *Nat. Catal.* **2019**, *2*, 198–210. [CrossRef]
113. Wuttig, A.; Yaguchi, M.; Motobayashi, K.; Osawa, M.; Surendranath, Y. Inhibited Proton Transfer Enhances Au-Catalyzed CO_2-to-Fuels Selectivity. *Proc. Natl. Acad. Sci. USA* **2016**, *113*, E4585–E4593. [CrossRef]
114. Yoo, J.M.; Ingenmey, J.; Salanne, M.; Lukatskaya, M.R. Anion Effect in Electrochemical CO_2 Reduction: From Spectators to Orchestrators. *J. Am. Chem. Soc.* **2024**, *146*, 31768–31777. [CrossRef] [PubMed]
115. Garg, S.; Li, M.; Wu, Y.; Nazmi Idros, M.; Wang, H.; Yago, A.J.; Ge, L.; Wang, G.G.X.; Rufford, T.E. Understanding the Effects of Anion Interactions with Ag Electrodes on Electrochemical CO_2 Reduction in Choline Halide Electrolytes. *ChemSusChem* **2021**, *14*, 2601–2611. [CrossRef] [PubMed]
116. Gao, D.; Scholten, F.; Roldan Cuenya, B. Improved CO_2 Electroreduction Performance on Plasma-Activated Cu Catalysts via Electrolyte Design: Halide Effect. *ACS Catal.* **2017**, *7*, 5112–5120. [CrossRef]
117. Yuan, X.; Ge, W.; Zhu, Y.; Dong, L.; Jiang, H.; Li, C. Anionic Surfactant–Tailored Interfacial Microenvironment for Boosting Electrochemical CO_2 Reduction. *ACS Appl. Mater. Interfaces* **2024**, *16*, 38083–38091. [CrossRef]